Direct drive: Simulations and results from the National Ignition Facility

P. B. Radha, M. Hohenberger, D. H. Edgell, J. A. Marozas, F. J. Marshall, D. T. Michel, M. J. Rosenberg, W. Seka, A. Shvydky, T. R. Boehly, T. J. B. Collins, E. M. Campbell, R. S. Craxton, J. A. Delettrez, S. N. Dixit, J. A. Frenje, D. H. Froula, V. N. Goncharov, S. X. Hu, J. P. Knauer, R. L. McCrory, P. W. McKenty, D. D. Meyerhofer, J. Moody, J. F. Myatt, R. D. Petrasso, S. P. Regan, T. C. Sangster, H. Sio, S. Skupsky, and A. Zylstra

Citation: Physics of Plasmas **23**, 056305 (2016); doi: 10.1063/1.4946023
View online: http://dx.doi.org/10.1063/1.4946023
View Table of Contents: http://scitation.aip.org/content/aip/journal/pop/23/5?ver=pdfcov
Published by the AIP Publishing

Articles you may be interested in

Low-adiabat rugby hohlraum experiments on the National Ignition Facility: Comparison with high-flux modeling and the potential for gas-wall interpenetration
Phys. Plasmas **21**, 112703 (2014); 10.1063/1.4901195

Hydrodynamic instability growth and mix experiments at the National Ignition Facilitya)
Phys. Plasmas **21**, 056301 (2014); 10.1063/1.4872026

Gain curves and hydrodynamic simulations of ignition and burn for direct-drive fast-ignition fusion targets
Phys. Plasmas **14**, 062701 (2007); 10.1063/1.2736947

High energy x-ray imager for inertial confinement fusion at the National Ignition Facility
Rev. Sci. Instrum. **77**, 10E301 (2006); 10.1063/1.2216996

Polar direct drive: Proof-of-principle experiments on OMEGA and prospects for ignition on the National Ignition Facilitya)
Phys. Plasmas **12**, 056304 (2005); 10.1063/1.1876252

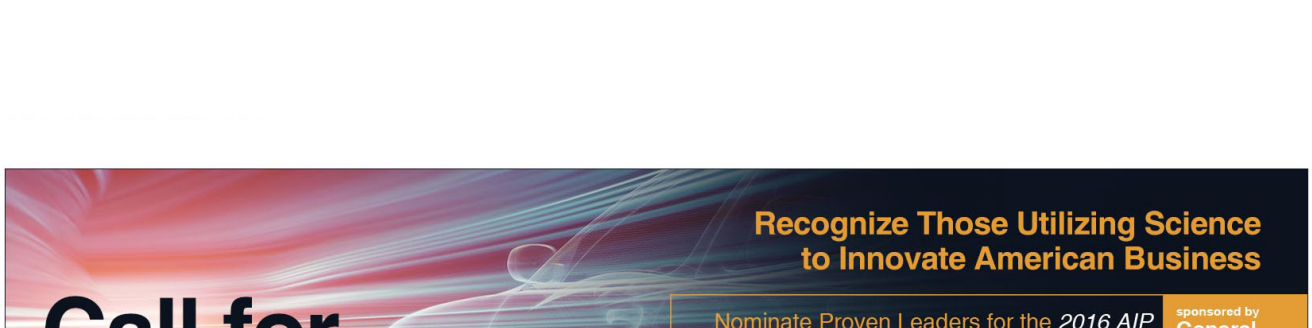

Reuse of AIP Publishing content is subject to the terms at: https://publishing.aip.org/authors/rights-and-permissions. Downloaded to IP: 198.125.179.176 On: Tue, 19 Apr 2016 16:35:07

Direct drive: Simulations and results from the National Ignition Facility

P. B. Radha,[1,a),b)] M. Hohenberger,[1] D. H. Edgell,[1] J. A. Marozas,[1] F. J. Marshall,[1] D. T. Michel,[1] M. J. Rosenberg,[1] W. Seka,[1] A. Shvydky,[1] T. R. Boehly,[1] T. J. B. Collins,[1] E. M. Campbell,[1] R. S. Craxton,[1] J. A. Delettrez,[1] S. N. Dixit,[2] J. A. Frenje,[3] D. H. Froula,[1] V. N. Goncharov,[1] S. X. Hu,[1] J. P. Knauer,[1] R. L. McCrory,[1] P. W. McKenty,[1] D. D. Meyerhofer,[4] J. Moody,[2] J. F. Myatt,[1] R. D. Petrasso,[3] S. P. Regan,[1] T. C. Sangster,[1] H. Sio,[3] S. Skupsky,[1] and A. Zylstra[3]
[1]*Laboratory for Laser Energetics, University of Rochester, Rochester, New York 14623, USA*
[2]*Lawrence Livermore Laboratory, Livermore, California 94550, USA*
[3]*Plasma Fusion Science Center, Massachusetts Institute of Technology, Cambridge, Massachusetts 02139, USA*
[4]*Los Alamos National Laboratory, Los Alamos, New Mexico 87545, USA*

(Received 6 January 2016; accepted 29 February 2016; published online 19 April 2016)

Direct-drive implosion physics is being investigated at the National Ignition Facility. The primary goal of the experiments is twofold: to validate modeling related to implosion velocity and to estimate the magnitude of hot-electron preheat. Implosion experiments indicate that the energetics is well-modeled when cross-beam energy transfer (CBET) is included in the simulation and an overall multiplier to the CBET gain factor is employed; time-resolved scattered light and scattered-light spectra display the correct trends. Trajectories from backlit images are well modeled, although those from measured self-emission images indicate increased shell thickness and reduced shell density relative to simulations. Sensitivity analyses indicate that the most likely cause for the density reduction is nonuniformity growth seeded by laser imprint and not laser-energy coupling. Hot-electron preheat is at tolerable levels in the ongoing experiments, although it is expected to increase after the mitigation of CBET. Future work will include continued model validation, imprint measurements, and mitigation of CBET and hot-electron preheat. *Published by AIP Publishing.* [http://dx.doi.org/10.1063/1.4946023]

I. INTRODUCTION

In direct-drive inertial confinement fusion,[1] nominally identical laser beams are incident on a capsule containing a layer of frozen deuterium-tritium (DT) within a shell made of an ablator such as plastic (CH). The beams ablate the outer material, driving the cryogenic DT layer inward. The shell accelerates during the laser pulse as a result of the pressure from the laser energy deposited in the corona and then decelerates when an outgoing shock is launched by the higher pressure in the vapor region compared to the inward moving shell. The shell kinetic energy is then converted to the internal hot-spot energy during stagnation. Ignition requires that the temperature and areal density of the hot spot should be sufficient to generate heating by the alpha particles produced from the D−T fusion reaction. Several measures of target performance have been presented in the literature.[2,3] The minimum fuel energy at ignition $E_{\min}$ considered here is given by[3]

$$E_{\min}(\mathrm{kJ}) = 50.8\alpha_{\mathrm{inn}}{}^{1.88}\left(\frac{V_{\mathrm{imp}}}{3\times10^{7}\,\mathrm{cm/s}}\right)^{-5.89} \times \left(\frac{P}{100\,\mathrm{Mbar}}\right)^{-0.77}, \quad (1)$$

where α_{inn} is the adiabat defined as the ratio of the pressure to the Fermi-degenerate pressure in the inner surface of the shell, V_{imp} is the implosion (peak) velocity of the shell, and P is the ablation pressure. Direct drive couples ∼3 to 5× more laser energy into the imploding shell than x-ray drive, resulting in larger values of V_{imp} for the same fuel mass and laser energy. As Eq. (1) indicates, for the same minimum energy for ignition, ignition designs with larger values of α_{inn} are possible in direct drive than in x-ray drive. Direct drive, for example, requires convergence ratios of ≳22 (defined as the ratio of initial radius to hot-spot radius at peak neutron production) to be ignition relevant, whereas x-ray drive requires convergence ratios of 30 to 40. Designs with higher adiabats are more robust to shock mistiming, preheat from fast electrons, or radiation. Higher-adiabat direct-drive designs also benefit greatly from reduced Rayleigh–Taylor (RT)[4] growth.[5] The high power of the velocity term in Eq. (1) also indicates that robust predictions of ignition require knowledge of the velocity of the shell to very high precision; a 5% decrease in velocity increases the minimum energy required for ignition by nearly 35%.

In direct drive, the implosion velocity and the ablation pressure are primarily determined by the coupling of the laser into the coronal plasma and the conduction of heat to the ablation surface. The equation of state has been shown to influence these quantities, although to a smaller extent.[6] While the dominant mechanism for laser energy absorption is collisional absorption (or inverse bremsstrahlung), because

Note: Paper CI3 4, Bull. Am. Phys. Soc. **60**, 59 (2015).
[a)]Invited speaker.
[b)]Author to whom correspondence should be addressed. Electronic mail: rbah@lle.rochester.edu

Reuse of AIP Publishing content is subject to the terms at: https://publishing.aip.org/authors/rights-and-permissions. Downloaded to IP: 198.125.179.176 On: Tue, 19 Apr 2016 16:35:07

of cross-beam energy transfer (CBET)[7] modifications in simulation codes are required to explain observables including capsule trajectory, scattered-light spectra and time histories, and bang times in OMEGA experiments.[8]

In CBET, ion-acoustic waves in the plasma mediate the transfer of energy from an incoming (pump) ray to an outgoing (probe) ray, reducing the energy available for deposition for the most hydrodynamically efficient incoming rays. The CBET gain factor scales as[7,8]

$$d\tau_{CBET} = f_{CBET}\zeta_{pol}\left(\frac{e^2}{c^3 m_e}\frac{n_e}{1-n_e}\frac{\lambda_0\langle Z\rangle}{\langle Z\rangle T_e + 3T_i}\right)P(\eta)I_{pump}ds, \tag{2}$$

where f_{CBET} is an ad hoc multiplier used to explore sensitivity to the model; $\zeta_{pol} = 1/4[1 + (\hat{k}_{pump} \cdot \hat{k}_{probe})^2]$ is the polarization factor; e is the electron charge; c is the speed of light; m_e and n_e are the electron mass and electron density, respectively; λ_0 is the laser wavelength; $\langle Z\rangle$ is the average ionization of the material; T_e and T_i are the electron and ion temperatures, respectively; $P(\eta) = \eta\nu_\alpha/[(\eta\nu_\alpha)^2 + (1-\eta)^2]$ is the resonance function with $\eta = [(\omega_{pump} - \omega_{probe}) - k_\alpha \cdot V_{fluid}]/|k_\alpha|c_\alpha$, where ω_{pump} and ω_{probe} are the pump and probe frequencies; k_α is the wave number of the ion-acoustic wave given by the wave-matching condition with sound speed c_α and the dimensionless ion-wave damping coefficient ν_α; and V_{fluid} is the fluid velocity. The model is limited by the assumption of a paraxial approximation which requires that the angle between the pump and probe beams be not too large. The energy gained or lost is modeled as $E_o(e^{d\tau_{CA}}e^{d\tau_{CBET}} - 1)$, where $d\tau_{CA}$ is the absorption factor caused by collisional absorption. This model has been implemented in the spherically symmetric code LILAC[9] and the axisymmetric code DRACO.[10] This CBET model has been compared to 60-beam OMEGA implosions and, at this time, an overall multiplier $f_{CBET} = 1.5$ is required in DRACO to reproduce the observed neutron rates and scattered light. The reason for an overall multiplier is unknown. It is speculated that the CBET model might have limitations because of the paraxial approximation and/or because of physics associated with the turning point of the rays. This fixed value of 1.5 is used in all of the OMEGA and NIF DRACO simulations described in this paper and used to compare to all the observables related to energetics available in the National Ignition Facility (NIF) experiments.

Differences between OMEGA[11] and National Ignition Facility (NIF)[12] scale implosions motivate the current experiments at the NIF. The simulated coronal temperature in NIF implosions is ~3.2 keV compared to ~2.75 keV in OMEGA implosions. Additionally, the path lengths for the rays, ds [Eq. (2)], in the NIF corona are significantly longer; the volume in the NIF corona is ~15 larger than OMEGA-scale implosions. Therefore, it is expected that the CBET effect will be considerably larger on the NIF scale. As will be shown later, for the ongoing experiments, CBET decreases implosion velocity by ~18% and the ablation pressure by ~57%, significantly increasing E_{min}. Validating such a model and demonstrating mitigation of CBET are important to the larger ignition program with direct drive.

The electron heat conduction from the laser-deposition region to the ablation surface sets up the ablation pressure in direct drive. Nonlocal heat conduction[13] has been shown to play an important role in shock timing in cryogenic DT OMEGA experiments and, in combination with CBET, is required to reproduce all observables related to energetics including trajectories, bang times, time-resolved scattered light, and scattered-light spectra. It is expected that nonlocal electron thermal transport should also play an important role in NIF-scale experiments.

Preheat from two-plasmon decay (TPD)[14] is expected to be larger on the NIF scale compared to OMEGA implosions. In TPD, plasma waves accelerate electrons to energies (≥30 keV) with sufficiently long mean free paths, so that their energy can be deposited in the cold shell, compromising compression or α_{inn}. TPD is a multibeam instability that requires the overlap of several beams to cooperatively overcome the threshold. In OMEGA implosions, the magnitude of the energy in the source of energetic electrons has been shown to scale with the threshold parameter η_{TPD}[14]

$$\eta_{TPD} = \frac{I_{n_c/4}\left(\times 10^{14}\,\mathrm{W/cm^2}\right)L_{n_c/4}(\mu\mathrm{m})}{233\,T_e(\mathrm{keV})}, \tag{3}$$

where, $I_{n_c/4}$, $L_{n_c/4}$, and T_e are the intensity, density scale length, and electron temperature at the quarter-critical surface, respectively. NIF implosions are characterized by higher coronal temperatures as mentioned earlier; however, the scale length is also larger—350 μm in the current experiments compared to 150 μm in OMEGA scale. Note that since the target sizes in the ongoing experiments are determined by the phase plates on the NIF, the scale lengths are smaller than those in ignition-relevant designs (~500 to 600 μm). The extrapolation to longer scale lengths suggests that a larger source of hot electrons is expected on the NIF. However, beam polarizations and beam angles also influence the extent of this instability. One significant difference between OMEGA and NIF experiments is that the ongoing NIF implosions are performed in the polar-direct-drive (PDD) geometry.[15] Beams displaced toward the equator to improve symmetry are incident at oblique angles onto the target. More beams are overlapped in the NIF geometry than OMEGA but with variations in the beam polarizations and incident angles. These differences motivate experiments on the NIF to estimate the TPD source and its effect on the imploding capsule.

This work describes the results from PDD implosions on the NIF. While a subset of results presented in this work has appeared previously,[16] a more-complete analysis including the validation of the CBET model in OMEGA PDD implosions, comparison of scattered-light spectra and time histories, and trajectories and shape of the imploding target with updated simulations that include a first-principles equation of state (FPEOS)[6] is presented here. This paper also includes a discussion of the reasons for possible differences between simulation and experiment.

The paper is organized as follows: The target design is discussed in Section II. Results from the experiments, organized by the physics topics—energetics and preheat—are

Reuse of AIP Publishing content is subject to the terms at: https://publishing.aip.org/authors/rights-and-permissions. Downloaded to IP: 198.125.179.176 On: Tue, 19 Apr 2016 16:35:07

discussed in Section III. Briefly, simulated scattered-light spectra show similar trends as observed; trajectories from backlit images and the shapes of the imploding core agree very well, although the trajectory from simulated self-emission images lags those from observations. Discussion of these results and sensitivity analyses to possible errors in CBET modeling, the effect of laser imprint, and fast-electron preheat are also presented in Section III. Future work is discussed in Section IV and conclusions are presented in Section V.

II. NIF TARGET DESIGN

The primary target type considered in this paper has an outer radius of ∼1100 μm with an ∼100-μm-thick, all-plastic (CH) shell filled with 20 atm of deuterium (D_2) gas [Fig. 1(a)]. The capsule is irradiated with a laser pulse shape whose temporal history includes a flat foot rising to a main pulse at varying laser intensities.[17,18] The shock launched during the foot of the pulse shape sets the implosion at an ignition-relevant adiabat α_{inn} ∼3. The implosions have a low convergence ratio of ∼13 (compared to 22 for direct-drive ignition), defined as the ratio of the initial radius of fuel–-shell interface to the final fuel radius at peak neutron production. The laser energy on target varies from ∼350 kJ (for a pulse shape with intensity $\sim 4 \times 10^{14}$ W/cm^2 at the initial target radius) to ∼650 kJ (corresponding to an on-target intensity of $\sim 1.2 \times 10^{15}$ W/cm^2). The pulse shapes are similar although they differ in the duration of the main pulse. The shell is deliberately set a low implosion velocity (compared to ignition-relevant values of 3.5×10^7 cm/s) between (1.8 and 2.2) $\times 10^7$ cm/s. The low velocity reduces the instability growth of the most-dangerous modes, which scale linearly with the implosion velocity.[19] This conservative design was chosen because the growth of single-beam nonuniformity (laser imprint) is expected to significantly compromise shell integrity in these implosions (also discussed in Section IV); the existing laser-beam smoothing is insufficient to drive high-performing implosions. Beam profiles used in the x-ray drive ignition campaigns[20] are used in the design. The on-target beam profile is calculated by forward propagating the near-field phase-front information using the code "*Waasikwa*."[21] The laser beams are defocused by 1 cm to improve the symmetry. This is taken into account in the calculation. Since only one set of near-field beam phase-front information is available for each cone, the same calculated profiles are used for all the beams within a cone.

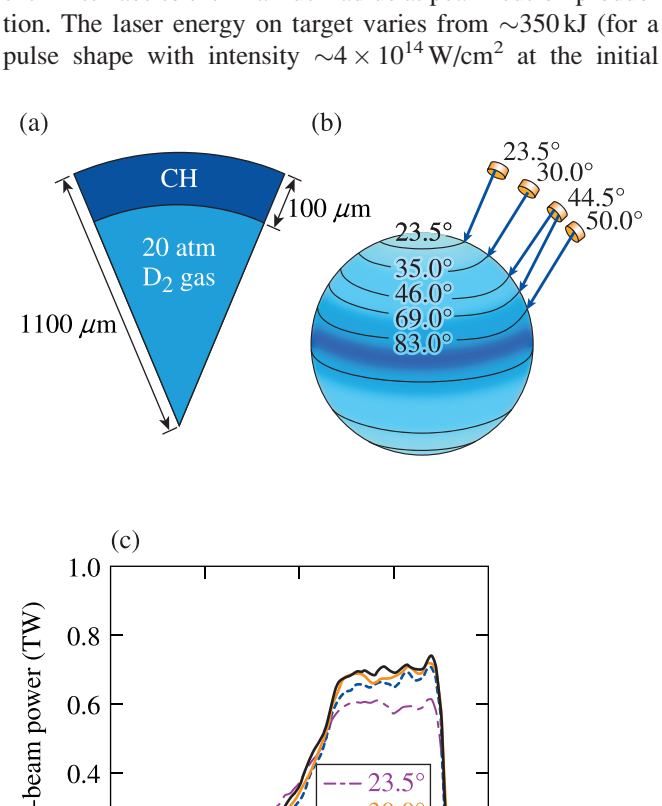

FIG. 1. (a) Schematic of the target used in a typical polar-direct drive (PDD) National Ignition Facility (NIF) implosion. (b) Pointing scheme in polar angle used for the PDD implosions. The four original cones at 23.5°, 30°, 44.5°, and 50° are repointed to the locations shown on the target. (c) Pulse shapes for each of the cones.

The beam geometry on the NIF is configured for the axisymmetric x-ray-drive configuration [Fig. 1(b)]. To improve irradiation symmetry, the equator requires additional drive. This is achieved by displacing the beams toward the equator as illustrated in Fig. 2. The beams on the NIF are arranged in cones at 23.5°, 30°, 44.5°, and 50°. In this PDD geometry, for example, the outer cone located at 50°, is displaced to irradiate the target at 83°. The beam configuration in Fig. 1(b) is obtained by iteratively adjusting the combination of beam displacements, beam defocus, and beam pulse shapes to reduce shell asymmetry.[17] In addition, beams in cones 44.5° and 50° are displaced azimuthally to improve the symmetry. Typical laser pulse shapes for the different cones are shown in Fig. 1(c). Notice that the 50° cone is driven with the highest power to provide additional drive in that region. The PDD configuration differs from the spherical-direct-drive (SDD) implosion studies on OMEGA,[17,22] where the models have been validated. The lack of drive at the equator is deliberately compensated for by displacing the beams toward the equator. These beams displaced toward the equator scatter around the target and, consequently, more scattered light appears near the poles in PDD than SDD. SDD is quasi-symmetric; simulations indicate that the scattered light around the target chamber varies by less than 1% rms (root mean square), significantly smaller than PDD. CBET, in particular, is influenced by the PDD beam displacements; more ray crossings occur over a region around the equator; therefore, CBET influences the laser-energy deposition in the region over the equator. As the schematic in Fig. 2(a) indicates, an outgoing ray (probe) from the southern hemisphere near the equator acquires energy from an incoming ray (pump) in the northern hemisphere and this excess energy in the outgoing ray can appear as scattered light over the northern polar region. This is also shown in Fig. 2(b) in the contour plot of the CBET energy gained per unit volume and normalized to the hydrodynamic time step. The contour plot shows the region where CBET dominates. Most of the energy gain in the rays occurs away from the

Reuse of AIP Publishing content is subject to the terms at: https://publishing.aip.org/authors/rights-and-permissions. Downloaded to IP: 198.125.179.176 On: Tue, 19 Apr 2016 16:35:07

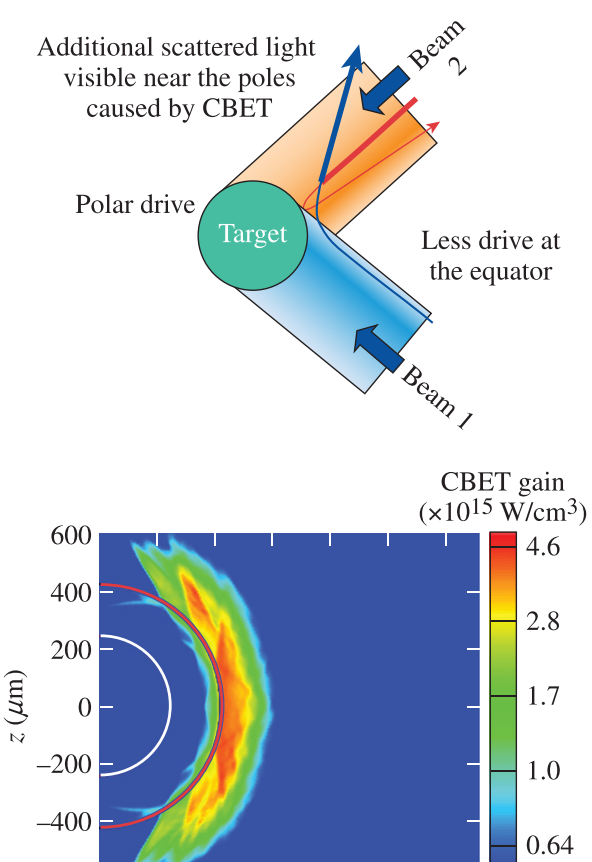

FIG. 2. (a) Schematic of cross-beam energy transfer (CBET) in the PDD geometry. The dominant transfer occurs when the energy is transferred from an incoming ray to an outgoing ray. (b) Contour plot of the energy gained from CBET. The transfer occurs away from the poles; more ray intersections occur away from the poles because of the PDD beam displacements.

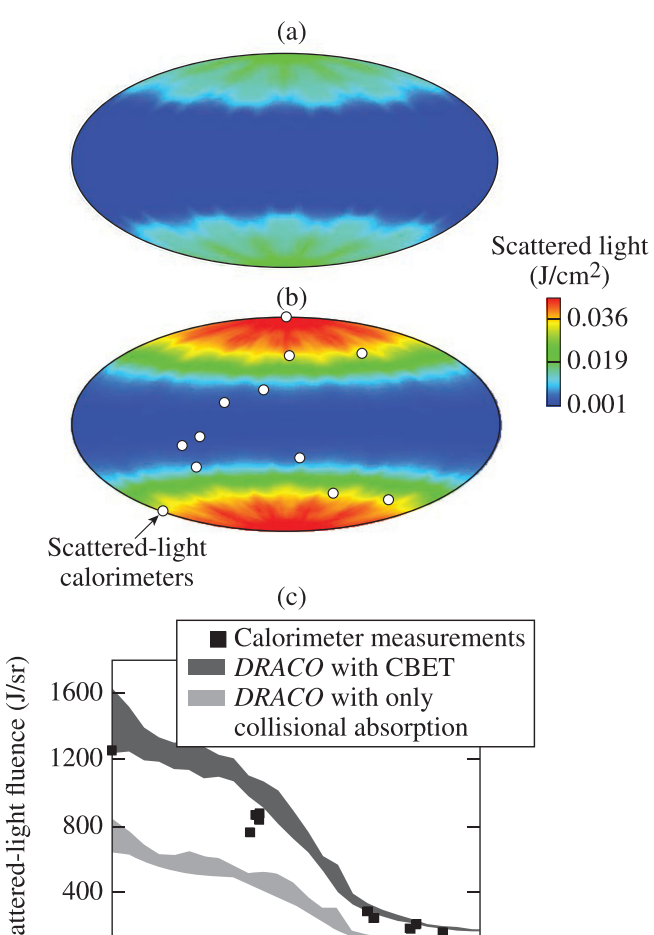

FIG. 3. Projected scattered light in the OMEGA target chamber from a simulation that includes (a) only the effect of collisional absorption and (b) the effect of CBET. Circles indicate the locations of the calorimeters in the OMEGA chamber. (c) Scattered-light fluence at the calorimeters in shot 64099 on OMEGA (symbols). The simulation is shown as a shaded region, indicating the minimum and maximum scattered light along the azimuthal angle. Light gray corresponds to Fig. 3(a)—only the effect of collisional absorption is included. Dark gray corresponds to Fig. 3(b)—the effect of CBET is also included in the simulation.

poles and in a range of polar angles closer to the equator. The projected scattered light around the target chamber is shown in Fig. 3 for an OMEGA PDD implosion. The hydrodynamic code *DRACO* with a full 3-D ray trace[23] that includes collisional absorption, nonlocal heat conduction,[24] and FPEOS[6] is used to simulate the PDD implosion. When the effect of CBET is included in the calculation [Fig. 3(b)], significantly more scattered light appears near the poles than when collisional absorption only is used to model the laser-energy deposition [Fig. 3(a)]. This has been observed in OMEGA PDD implosions. Scattered-light flux around the target chamber as a function of polar angle, collected using calorimeters in a PDD implosion irradiated with a similar pulse shape as the NIF implosions,[25] is shown in Fig. 3(c). The location of the calorimeters is shown as circles in Fig. 3(b). As the figure indicates, significantly more scattered light appears near the poles when CBET is included in the calculation (dark gray) compared to when only collisional absorption is included (light gray). The shaded region indicates the minimum and maximum light along the azimuth as calculated by the 3-D ray trace. The additional polar light agrees well with the observations (symbols), which also show the same trend.

Simulations indicate that the energy transfer from the incoming rays occurs at the center of the beam for rays with the smallest incident angles that are the most hydrodynamically efficient. This results in less drive around the equatorial region. Therefore, CBET makes the implosion more oblate than collisional only absorption as seen by the synthetic self-emission images of the imploding shell (Fig. 4). Requiring simulations to reproduce the observed shape of the imploding core, i.e., the drive as a function of polar angle, makes PDD a more-stringent test of direct-drive implosion physics than SDD.

III. RESULTS AND DISCUSSION

A. Energetics

1. Results

Energetics on the NIF is inferred from time-resolved scattered light measured using fast diodes[26] and a streak

Reuse of AIP Publishing content is subject to the terms at: https://publishing.aip.org/authors/rights-and-permissions. Downloaded to IP: 198.125.179.176 On: Tue, 19 Apr 2016 16:35:07

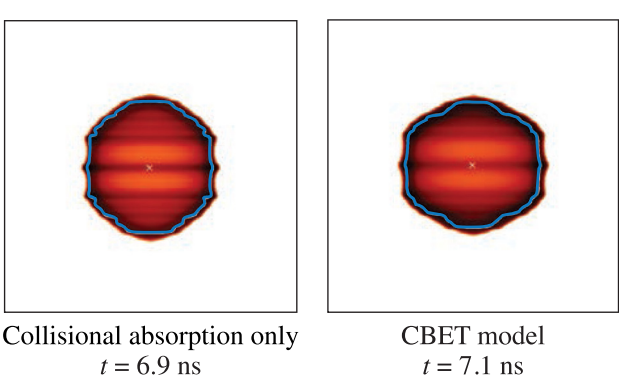

FIG. 4. Simulated self-emission images from N150118-002 with (a) only collisional absorption laser deposition included in the calculation and (b) the effect of CBET also included in the calculation.

camera.[26] The time-resolved scattered light is plotted in Fig. 5. The simulation tracks the observations very closely with deviations between 5 and 7 ns. The implication of the excess simulated scattering is unclear. Additional information is also available from the two full-aperture backscatter stations (FABS)[26] that measure the spectrum of scattered light. Fig. 6(a) shows the spectra observed by the FABS. Features characteristic of implosions are observed in the spectra: a rapid blue shift is observed early in time corresponding to corona formation; the red-shift at ~2 ns corresponds to the onset of inward motion of the corona during the acceleration phase. Very similar trends are observed in the *DRACO* simulation [Fig. 6(b)]. Similar agreement is obtained with the spectra from the other FABS location. Quantitative inferences of the energy in the scattered-light spectrum and the time-resolved light are in progress and are important to further validate the modeling (discussed in Section IV).

Trajectories of the converging shell provide information about the laser energy coupled to the target and are measured in two ways: the first uses gated framing cameras to measure the self-emission of the target[27] using a 1-mil-thick Be filter (~25 μm) corresponding to photon energies $\gtrsim$1 keV and the second uses a gated framing camera to measure a radiograph obtained by backlighting an implosion[28] using Fe (~6.7 keV).

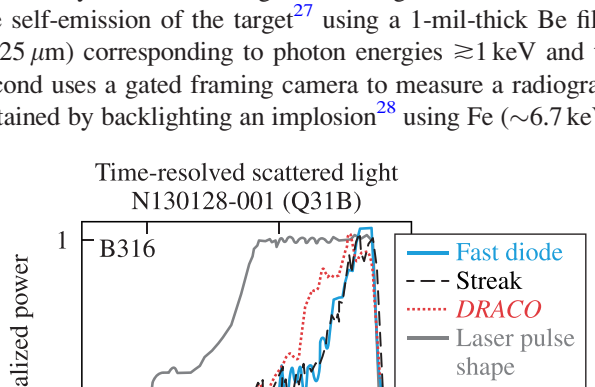

FIG. 5. Time-resolved scattered light measured at one location corresponding to B316 from fast diodes and optical streak cameras (dashed-dotted and solid lines). Time-resolved scattered light from a simulation including the effect of CBET is also shown (dashed line).

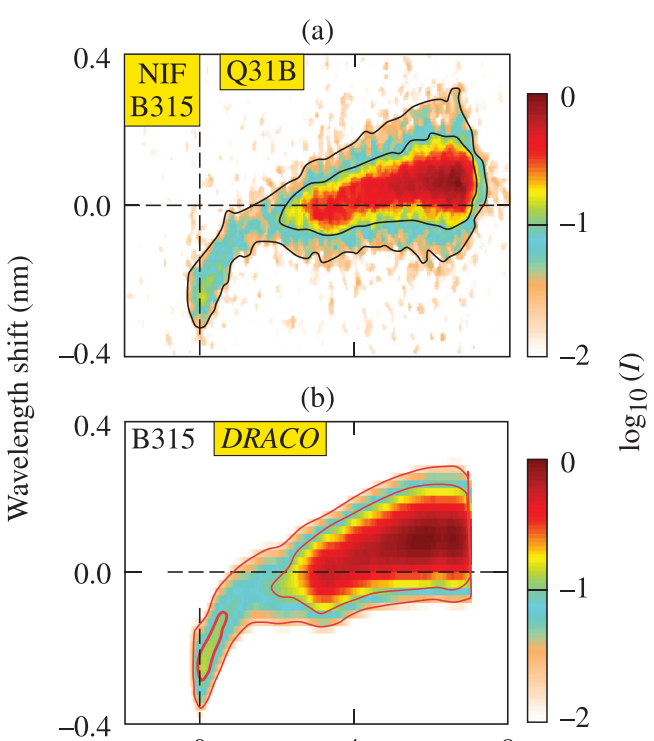

FIG. 6. Scattered-light spectrum measured using the full-aperture backscatter station (FABS) diagnostic at one location and corresponding to same location as the diodes. (a) Measured scattered-light spectrum and (b) spectrum from a simulation including the effect of CBET.

Excellent agreement is obtained with the CBET model on OMEGA to replicate observed trajectories from self-emission images,[22] while trajectories from backlit images have been explored to a more-limited extent.[28] The design for a backlit implosion requires changes to the beam configuration. Two quads (one from each hemisphere) are removed to irradiate an iron backlighter. The energies of eight neighboring quads and their pointing are adjusted to improve symmetry. Figure 7 shows typical images obtained from the framing cameras. The

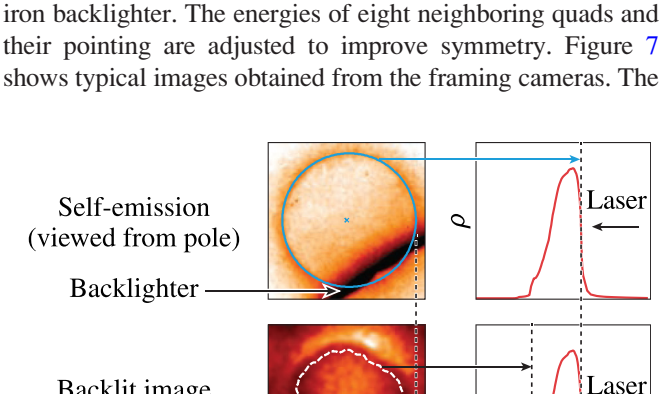

FIG. 7. Typical self-emission image viewed from the pole and backlit image viewed from the equator from shot N140612-001. Absorption images are obtained at 6.7 keV by backlighting the implosion with Fe. Self-emission images are viewed at 1 keV with a Be filter of 1 mil thickness. The lineouts point to the surfaces in the density profile (right) that are extracted from the image.

Reuse of AIP Publishing content is subject to the terms at: https://publishing.aip.org/authors/rights-and-permissions. Downloaded to IP: 198.125.179.176 On: Tue, 19 Apr 2016 16:35:07

view from the pole records the self-emission [Fig. 7(a)]. Simulations indicate that the location of the steepest gradient corresponds closely to the ablation surface.[27] This location is indicated on a typical simulated density profile of the implosion. Notice the circular polar image indicating that the nonuniformity imposed by the removal of quads to irradiate the backlighter has been adequately compensated by the increased energies and repointing of the eight neighboring quads. The view from the equator records the backlit image [Fig. 7(b)]. The surface of the greatest absorption corresponds to the location of the fuel–shell interface as indicated by the same density profile. Therefore, the difference in the location of the two surfaces can be interpreted as the thickness of the imploding shell.

Trajectories for different shots are plotted in Fig. 8. Simulations are post-processed using the code *Spect3D*[29] to create the self-emission and backlit images. The finite spatial resolution (~20 to 30 μm pinhole size depending on the shot) and gating time window of the cameras (~100 ps) are included in the simulated images. The same analysis is used to extract average radii from the synthetic and measured images.[27,28] The solid line from the backlit image reproduces the inferred trajectory very well, whereas the dashed line from self-emission images apparently overestimates the drive. The slopes of the two trajectories indicate that the velocity inferred from the backlit images is reproduced within 1% by the simulation, whereas the velocity inferred from the self-emission images is overestimated by ~9%. If the self-emission trajectory was representative of the

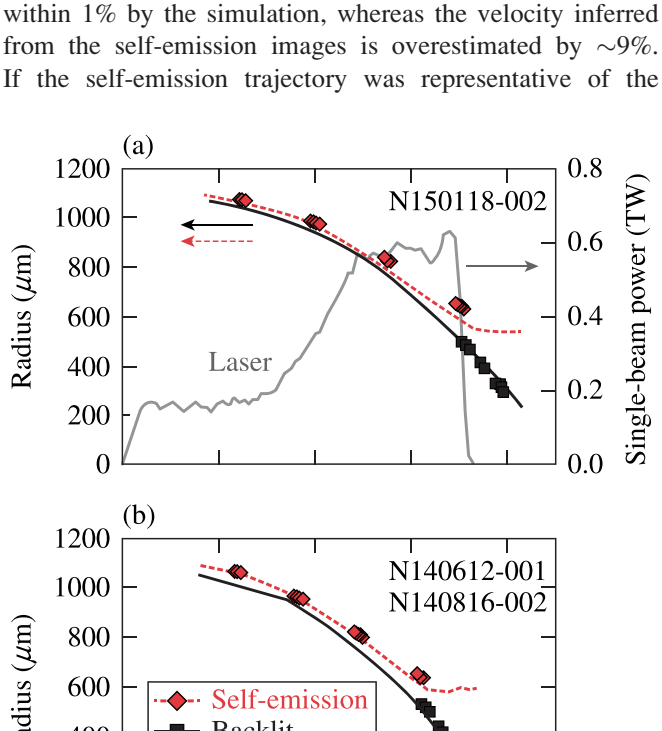

FIG. 8. (a) Trajectories from backlit images from measurements (squares) and simulations (solid line). Trajectories from self-emission images from measurements (diamonds) and simulations (dashed line) for shot N150118-002. (b) same as (a) but for shots N140612-001 and N140816-002.

velocity, this would significantly increase E_{min}, compromising ignition. It is therefore important to resolve the difference and identify which trajectory, if either, is representative of the true implosion velocity. Note that the inferred shell thickness estimated using the procedure in Fig. 7 is larger than the simulated value. The trajectories and shell thickness can be influenced by several factors including errors in one-dimensional (1-D) modeling such as errors in the energy coupling models, preheat (radiative or fast electron), and multidimensional physics such as Rayleigh–Taylor growth seeded by imprint. It is important to understand if the differences are caused by errors in the 1-D modeling since they influence models used to predict ignition. If imprint was the cause, it is expected to be of less concern as improved beam smoothing[30] and target designs with doped-CH overcoat[31] or Au layers[32] have been shown to mitigate this effect. Each of these factors is first discussed below. The results are first discussed qualitatively and then collated in a plot showing the relative magnitude of each of these effects.

2. Sensitivity analysis

Overestimating the predicted velocity of the early shock (resulting from inaccuracies in the modeling of laser coupling or equation of state) can delay the trajectory. If the shock was slower than simulated, the breakout of the shock into the gas would be delayed, postponing the onset of acceleration. Shock mistiming can thicken the converging shell: a higher adiabat results in a lower-density shell that occupies a larger volume during convergence. However, for this pulse shape, the absorption during the low-intensity foot is very high (~95%). The mechanism for absorption during this time is primarily collisional absorption. Therefore, any mistiming of the shock is small and its effect on shell thickness and trajectory is insignificant. For example, mistiming the shock during the foot by using a flux-limited diffusive heat-conduction model with flux-limiter $f = 0.06$ (Ref. 33) instead of the nonlocal transport delays the shock breakout by less than 20 ps, which only marginally influences trajectory and shell thickness. It is therefore hypothesized that the observations cannot be explained by shock mistiming alone.

Sensitivity analysis to the CBET model is examined using the spherically symmetric code *LILAC* by using a multiplier, $f_{CBET} = 2$ in the gain factor [Eq. (2)]. Figure 9 shows the density profiles at different times in the simulation of an NIF-type implosion when the inner surface of the shell has traveled the same distance. The shell becomes increasingly decompressed and the ablation pressure is reduced as the extent of CBET is increased in the modeling (Table I). This also significantly reduces the absorption fraction, suggesting that a detailed quantification of the scattered light is crucial to achieve higher accuracy in the laser-deposition CBET modeling. The implosion velocity, which decreases as the extent of CBET increases in the model, is also listed in Table I. This is also shown in Fig. 10 through the trajectories of the two surfaces; CBET reduces the velocity of both the surfaces while decompressing the shell. Agreement with the experimentally inferred trajectories requires that the backlit trajectory remains unchanged, whereas the self-emission

Reuse of AIP Publishing content is subject to the terms at: https://publishing.aip.org/authors/rights-and-permissions. Downloaded to IP: 198.125.179.176 On: Tue, 19 Apr 2016 16:35:07

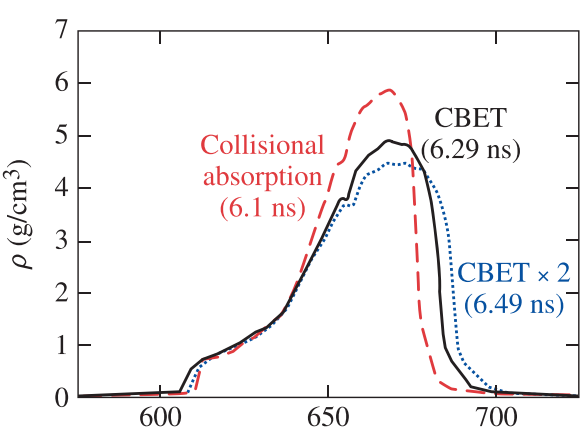

FIG. 9. Density profiles showing the sensitivity of the shell thickness to different extents of CBET (dashed: collisional absorption only; solid: CBET with $f_{\mathrm{CBET}} = 1$; dotted: CBET × 2 with $f_{\mathrm{CBET}} = 2$).

trajectory becomes apparently slower. Therefore, an error in the CBET modeling alone is insufficient to explain the observation.

Preheat from energetic electrons can also potentially influence the trajectories. The energy in energetic electrons is inferred in NIF implosions through the filter-fluorescence x-ray (FFLEX)[34] diagnostic. FFLEX measures the time-resolved x-ray emission in ten channels ranging from ∼20 keV to 250 keV. The inferred total cumulative energy E_{hot} is calculated assuming that the entire observed x-ray emission is from the deposition of the fast-electron energy in the CH ablator. A value of $E_{\mathrm{hot}} \sim 2.5 \pm 0.3$ kJ is therefore obtained corresponding to ∼0.4% of the total laser energy. The hot-electron temperature is inferred by fitting the measured time-integrated x-ray spectrum for the various FFLEX channels. The fit yields a value of 46 ± 3 keV for the shots considered here.[16] This is consistent with temperature measurements on OMEGA.[35] A straight-line deposition formula is used in *LILAC* to simulate the effect of this distribution of electrons on the trajectory and shell thickness.[36] A wide angular divergence of the electrons (240°) is assumed in the model. Studies of TPD in SDD OMEGA implosions using Mo balls of different radii suggest that the electrons are produced at a large divergence angle.[35] Indications of isotropy were also observed in NIF PPD implosions in the DIME (defect-induced mix experiment) campaign.[37] Energetic x-rays produced in the DIME NIF PDD implosions are observed via pinhole images and are also isotropic.[38] Therefore, a straight model in the spherically symmetric

TABLE I. The effect of important implosion parameters with increasing extents of CBET using the spherically symmetric code *LILAC*. CBET × 2 corresponds $f_{\mathrm{CBET}} = 2$ in Eq. (2). The numbers in parentheses indicate the values (in %) of the quantity relative to the collisional absorption value.

Model	P_{abl} (Mbar)	M_{abl} ($\times 10^6$ cm/s)	V_{imp} ($\times 10^7$ cm/s)	f_{abs} (%)
Collisional absorption	70	1.4	2.2	95
CBET	30 (43%)	0.8 (57%)	1.8 (82%)	75 (79%)
CBET × 2	15 (21%)	0.6 (43%)	1.5 (68%)	64 (67%)

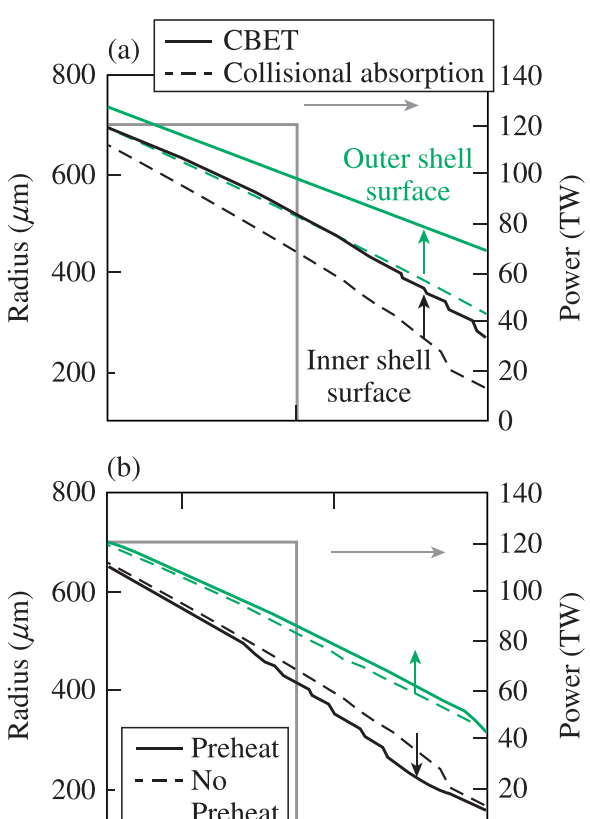

FIG. 10. Dependence of the backlit and self-emission trajectory to models with (a) collisional absorption only (dashed lines), including the effect of CBET (solid lines), and (b) collisional absorption only (solid line), including the effect of preheat (dashed line). The laser pulse, corresponding to the right axis, is shown for reference.

code *LILAC* is expected to reproduce the sensitivity of the NIF implosion to fast-electron preheat. The observed time-resolved history of the x-ray emission (Fig. 13 in Ref. 15) is calculated by the model—almost no emission is observed until ∼4 ns. The emission then increases during the main pulse and stops at approximately the end of the laser pulse. The effect of these electrons on the implosion is shown in Fig. 10. A factor of ∼2 more electron energy (4.6 kJ) than experimentally inferred is required in the simulation to make the effect more visible on the plot. Preheat increases the shell thickness and decreases the slope of the self-emission trajectory as required to match the observations. However, note that it also increases the slope of the backlit trajectory contrary to what is required to match the observations. The significantly larger magnitude of the preheat source required to observably change trajectories and shell thickness suggests that preheat alone is likely not the cause for the observed discrepancies between simulation and measurements. A comparison of the simulated and inferred self-emission trajectory from a low-intensity shot ($\sim 4 \times 10^{14}$ W/cm^2 at the initial target radius) also indicates the apparent slowing down of the self-emission trajectory (Fig. 11). At this intensity, the energy in fast-electrons is estimated to be less than 0.05% of the laser energy at the noise level of the FFLEX instrument—a value that has an insignificant effect on the implosion. This

Reuse of AIP Publishing content is subject to the terms at: https://publishing.aip.org/authors/rights-and-permissions. Downloaded to IP: 198.125.179.176 On: Tue, 19 Apr 2016 16:35:07

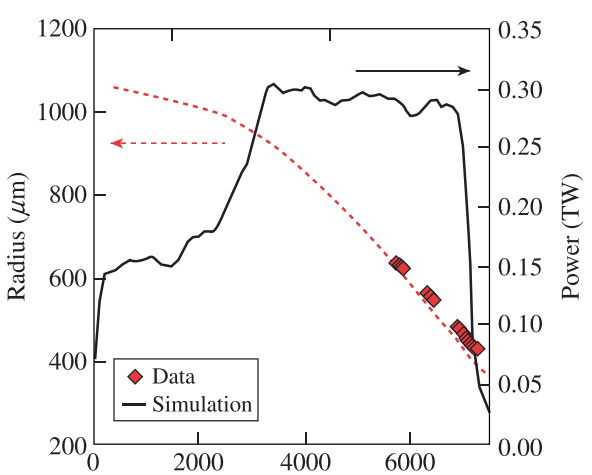

FIG. 11. Trajectories from a low-intensity ($\sim 4 \times 10^{14}$ W/cm^2 average on-target intensity at the initial target radius) implosion, N130128-001. Only self-emission trajectory is measured for this shot (diamonds). The simulated trajectory, including the effect of CBET, is shown as a solid line.

also suggests that fast-electron preheat is less likely a cause for the apparent shell decompression. Fast-electron preheat can be conclusively ruled out only if the backlit trajectory is also well reproduced at the low intensity and the trend in the discrepancy at the two different intensities stays the same. This is being investigated with a low-intensity implosion where a backlit trajectory is also available.

Finally, we discuss multidimensional effects. Single-beam laser nonuniformity imposes nonuniformity on the target starting at short wavelengths corresponding to $\sim 10\,\mu$m ($\lambda \sim 600$ at the initial target radius).[10] The effect of laser imprint and the subsequent RT growth is modeled using *DRACO*. Density contours at the end of the acceleration phase for an NIF implosion is shown in Fig. 12. To make the simulation tractable, only modes up to $\lambda \sim 200$ are included in the calculation. The shell is significantly distorted with a relatively intact inner shell. Trajectories from simulated images (Fig. 12) indicate that the backlit trajectory is unchanged relative to a simulation with no distortions, whereas the self-emission region moves further outward, leading to an apparent decompression of the shell. This trend is consistent with experiments. A larger-scale simulation including modes up to $\lambda \leq 600$ is being performed to study the influence of shorter wavelengths on the trajectory and shell thickness. Of the three sources of modeling uncertainty considered so far, only laser imprint shows the correct trends of keeping the backlit trajectory relatively unchanged and causing an apparent slowing down of the self-emission trajectory.

The results from these sensitivity studies are summarized in Fig. 13. The percentage increase in shell thickness over the nominal implosion (defined as including: CBET, nonlocal transport, and FPEOS) is plotted against the percentage of preheat energy in the fast-electrons source. To explore the sensitivity to angular divergence, electrons are launched isotropically with an angular divergence of 240°. Shell thickness increases slowly with increasing preheat. The observed shell thickness, shown for two shots, is

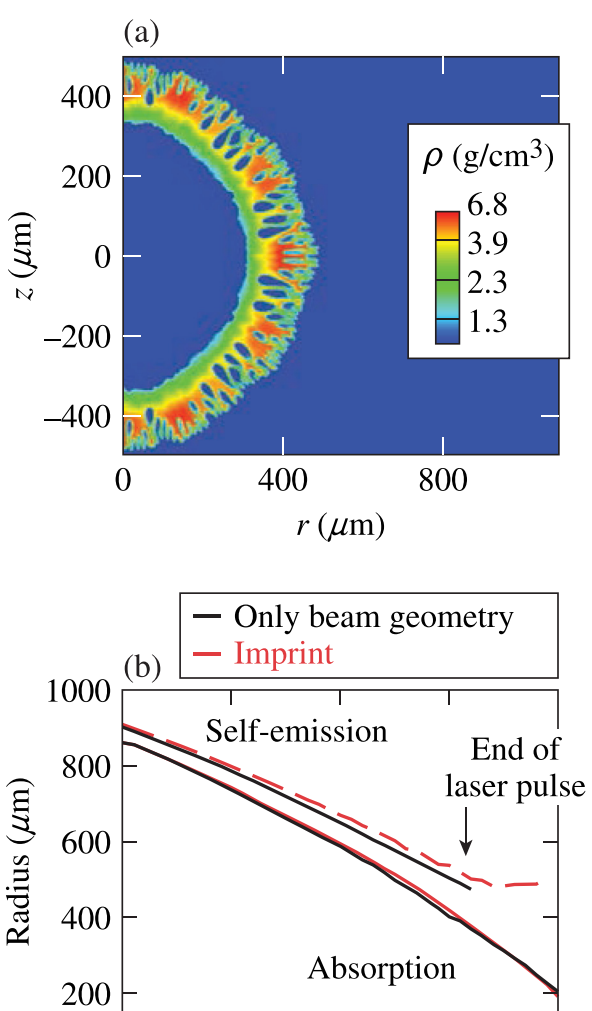

FIG. 12. The effect of single-beam nonuniformity (laser imprint) is shown as (a) density contours at the end of the acceleration phase.(b) Trajectories extracted from post-processed synthetic images of the simulation shown in (a).

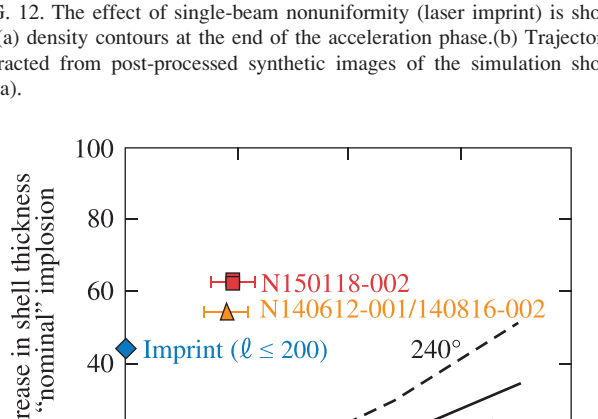

FIG. 13. Increase in shell thickness (in %) over the nominal implosion defined as one including the effects of CBET, FPEOS, and nonlocal transport. The symbols with error bars correspond to measured values from framing-camera images. The lines correspond to the simulated effect of preheat. The circle shows the effect of $f_{\mathrm{CBET}} = 2$ in the CBET model. The effect of imprint is shown (diamond).

Reuse of AIP Publishing content is subject to the terms at: https://publishing.aip.org/authors/rights-and-permissions. Downloaded to IP: 198.125.179.176 On: Tue, 19 Apr 2016 16:35:07

significantly higher than the increase caused by preheat, indicating that preheat alone is insufficient to explain the observed thickness. The increase in thickness from $f_{\mathrm{CBET}} = 2$ is also shown in Fig. 13. The relatively small change in shell thickness resulting from any possible error in the CBET model also suggests that energetics is well modeled and is likely not the cause for the observed differences. The increase in shell thickness caused by imprint is shown in Fig. 13. Of all the sources considered, imprint is the dominant contributor to the increase in shell thickness. Imprint also leaves the backlit trajectory unchanged, which is required for consistency with the measurements. It is hypothesized that some combination of the various sources of error and imprint will explain the observations with imprint as the dominant source.

A further indication that the laser drive is well modeled is obtained from the shape of the imploding core. Simulated and observed backlit images are shown in Fig. 14 for approximately the same convergence. Note that the shapes are far from round. This is a limitation of the available beam profiles on the NIF. Significantly improved implosions can be obtained with custom beam profiles.[39] The observed shape is very well reproduced by simulations. This is quantified by the radial deviation about the mean radius in Fig. 14(c), where the observed and simulated lineouts of the radial deviation are overlaid. Excellent agreement is obtained, suggesting that the energetics is well modeled. Small deviations are observed near the pole. This difference is also observed on a lower-intensity shot (Fig. 15). The measured and simulated images at the low intensity show reasonable agreement in

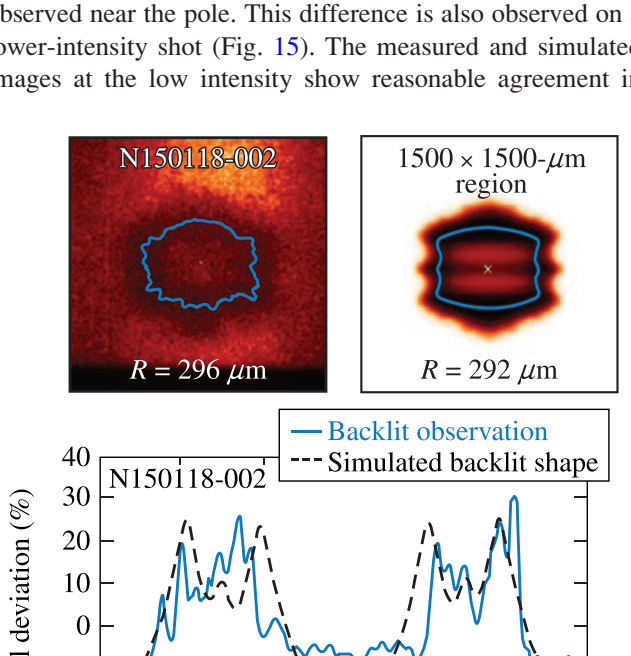

FIG. 14. (a) Measured backlit image using the Fe line at 6.7 keV. The line indicates the surface of maximum absorption. (b) Simulated backlit image. Line shows the surface of maximum absorption. Bottom: Lineout in polar angle of the radial deviation about the mean at approximately the same convergence for measurements (solid) and simulations (dashed) for shot N150118-002.

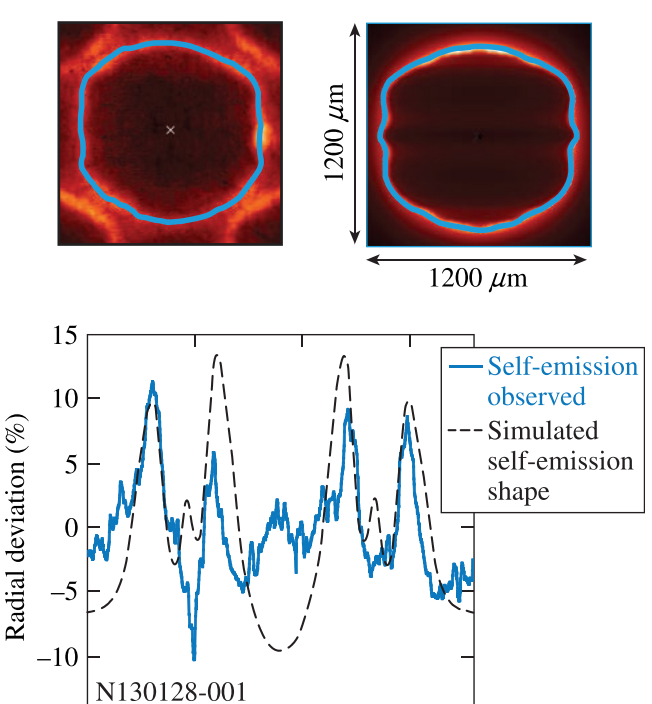

FIG. 15. (a) Measured self-emission image. The line indicates the surface of steepest gradient of emission. (b) Simulated image. The line shows the surface of maximum absorption. (c) Lineout in polar angle of the radial deviation about the mean at approximately the same convergence for measurements (solid line) and simulations (dashed line) for shot N130128-001.

the shape [Figs. 15(a) and 15(b)]. The deviation of the lineout about the average radius versus polar angle is shown in Fig. 15(c). The gross shape is well reproduced, although the polar region is driven significantly more in the simulation compared to experiment. Since this difference is systematic between two shots, a plausible reason for this difference could be an incomplete knowledge of the calculated defocused beam profiles. No measurements of these profiles are available at this time. Moreover, as mentioned earlier, while different beam profiles are calculated for each cone, the same profile is used for all the beams within the cone. Beam-to-beam variations are not included in the calculation since this information is unavailable.

3. Preheat

Estimates from FFLEX measurements in NIF implosions indicate that ~0.4% of the laser energy is converted into electron energy at intensities 8×10^{14} W/cm^2 (the lowest ignition-relevant intensity).[16] Preheat results inferred from FFLEX for shots with varying intensity are summarized in Fig. 16. In integrated implosion experiments, typically only the preheat source is inferred from the measurement of bremsstrahlung x-rays emitted by the fast electrons. The energy deposited in the cold shell, which is the relevant quantity for designs, is usually calculated using models[36] or estimated from complementary experiments.[40] It has been shown previously from semi-analytic estimates that ignition fails if 1.5% of the shell kinetic energy is deposited as the

Reuse of AIP Publishing content is subject to the terms at: https://publishing.aip.org/authors/rights-and-permissions. Downloaded to IP: 198.125.179.176 On: Tue, 19 Apr 2016 16:35:07

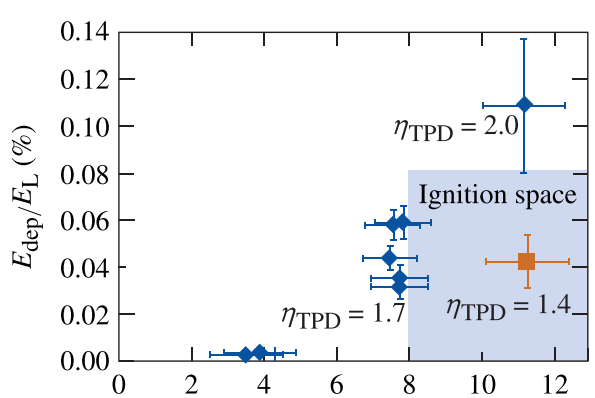

FIG. 16. Estimated deposited energy from energetic electrons from two-plasmon–decay (TPD) as a fraction of the total laser energy versus the polar-angle averaged on-target laser intensity during the peak of the laser pulse (measured at the initial target radius) for CH ablators (diamonds) and a target with an outer Si layer (square). The shaded region shows the range of acceptable preheat from fast electrons.

preheat energy into the shell.[41] A typical ignition design at 1.5 MJ of laser energy, with ~80 kJ of shell kinetic energy, can tolerate a maximum of 1.2 kJ or 0.08% of the laser energy deposited in the cold shell without compromising ignition significantly. A similar fraction of ≲1% of the laser energy deposited in the cold shell has been previously obtained from *LILAC* simulations.[42]

The deposited energy in experiments described in this work is estimated using OMEGA implosions. A combination of room-temperature and cryogenic implosions of equivalent mass has been used to infer the energy deposited in the cold shell.[40] This work estimates that ~1/7th of the electron source energy is deposited in the high-density shell. This result is applied to the NIF implosions to estimate the energy deposited. The preheat value in Fig. 16 is the estimated value from the measurement of the preheat source in NIF experiments divided by this factor as a fraction of the total laser energy. The shaded region in the figure shows the acceptable range of intensity and deposited energy based on the analysis presented above. The preheat scales with the calculated values for the threshold parameter, η_{TPD}, consistent with OMEGA implosions. The figure shows that preheat for CH ablators is tolerable at intensities closer to 8×10^{14} W/cm^2, whereas it is clearly at an unacceptable value for ignition at higher intensities. Simulations indicate that with full CBET mitigation, $I_{n_c/4}$ will increase by nearly 60%, raising the value of η_{TPD} to 2.6 at an intensity of 8×10^{14} W/cm^2. This will likely result in greater preheat and a value possibly closer to the currently observed estimate at the higher intensity of 1.2×10^{14} W/cm^2. This would result in a failure of ignition.

The presence of a mid-*Z* layer such as Si at the quarter-critical surface during the time of TPD production (the latter part of the main pulse) (Fig. 13 in Ref. 15) has been shown to reduce the preheat source in OMEGA implosions.[43] The reduction in the preheat source is primarily from the higher temperature in the corona because of the high atomic number of Si. A similar NIF experiment with an outer 14 μm of Si overlaid on a CH layer is also shown in Fig. 16. In this design, Si is present in the quarter-critical surface throughout the implosion. For this implosion, the temperature in the corona increases from 3.5 keV to 4.5 keV, reducing η_{TPD} from 2.0 to 1.4. This reduces the shell preheat to tolerable levels. A similar implosion will be repeated after CBET mitigation to study mitigation of fast-electron preheat.

IV. FUTURE WORK

Future work related to NIF experiments will include continued model validation. As mentioned earlier, quantification of scattered light is important to disentangle the various effects discussed above and could potentially explain the discrepancy in the self-emission trajectories. Further validation requires larger-scale imprint simulations to isolate the effect of imprint. Measurements of imprint in cone-in-shell geometry[44] will be performed over the next year on the NIF. These experiments will also serve as platforms for future studies of imprint and its mitigation when improved beam smoothing[30] is installed on the NIF. As Table I shows, CBET decreases the mass ablation rate and the implosion velocity. Mitigation of CBET is important to recover robust ignition designs. As Eq. (2) shows, detuning the wavelengths of the pump and probe beams will detune the resonance and reduce the volume over which CBET can occur, reducing the magnitude of the effect. This will be studied using the available tunable wavelength capability of the NIF: a maximum of ±2.3 Å in the UV.[45] This value is smaller than what is required to recover more than 50% of the CBET energy lost in simulations (6 Å in the UV).[45] However, simulations predict that differences in the shape, trajectory, and the magnitude of scattered light should be observable in the experiment.[45] Other means to improve mass ablation rates such as Be ablators[46] will be explored in the coming year. Finally, TPD mitigation will be studied with a mid-*Z* layer such as Si after CBET has been mitigated.

The longer-term pre-ignition goal on the NIF is to implode a multilayer target such as the one described in Ref. 22. A mass-equivalent CH layer will replace the cryogenic DT layer in the room-temperature equivalent of the cryogenic target described in Ref. 22. A multilayer target will permit imprint mitigation (though the use of doped ablators such as CHSi or Au layers), the reduction of TPD through the use of a thin Si layer that would be present at the quarter-critical surface only during the latter part of the main pulse (where TPD is evident from fast electrons), and a Be layer to provide improved mass ablation rate. A high-convergence implosion is not expected from this design since the outer layers of Si radiatively preheat the inner CH layer. This effect is small when a DT layer is used instead because of its low opacity. High-convergence direct-drive NIF implosions with CBET and TPD mitigation are possible only in cryogenic DT layered targets.

Ignition attempts require additional investments in hardware on the NIF including improved beam smoothing,[30] custom phase plates,[39] cryogenic target layering, and delivery systems. At this time, it is unclear if such an attempt would involve SDD or PDD. A study in this year will explore the

Reuse of AIP Publishing content is subject to the terms at: https://publishing.aip.org/authors/rights-and-permissions. Downloaded to IP: 198.125.179.176 On: Tue, 19 Apr 2016 16:35:07

facility and mission impacts of moving some of the NIF beams to enable spherical illumination. The NIF target chamber has ports for such beam placement. The results presented in this work apply to either scheme. Estimating imprint, the effect of laser–plasma interactions at long scale lengths on implosions and their mitigation is a critical component of studying the viability of direct drive as an ignition option.

V. CONCLUSIONS

Results from NIF PDD implosion experiments are presented. The goal is to test the modeling of energetics and measure the extent of preheat in NIF implosions that have longer coronal density scale lengths than comparable implosions at the Omega Laser Facility. Observables such as the shape of the scattered-light spectrum, time-resolved scattered light, trajectories from backlit images, and the shape of the imploding shell agree very well with *DRACO* simulations. However, the trajectory from self-emission images lags simulations, suggestive of a slower trajectory from self-emission or a thicker shell than simulated. While the cause for this discrepancy is unknown, sensitivity analyses for the various effects that might result in an effectively decompressed shell indicate that errors in modeling of the energetics, such as those in the CBET model, are likely not the cause. Laser imprint and subsequent Rayleigh–Taylor growth appear to be the dominant source of the observed difference. The CBET model that best reproduces the observations requires the same overall multiplier to the gain factor for both OMEGA and NIF simulations. It is expected that quantifying the scattered light in the NIF experiments will help identify if this is indeed the case and further test model predictability. The fast-electron preheat source in ongoing implosions is at a tolerable level ($\sim$0.4% of laser energy at an ignition-relevant intensity of 8×10^{14} W/cm^2 at the initial target radius) corresponding to $\sim$0.06% of the energy deposited in the cold shell. While this is believed to be tolerable for ignition, it is expected that with the mitigation of CBET, the preheat source will increase, leading to more energy deposited in the cold shell. Implosions with mid-*Z* layers have been shown to reduce the preheat source (by nearly a factor of 3). Future pre-ignition plans on the NIF include continued validation of models through measurements of imprint, mitigation of CBET, and TPD. All of these mitigation strategies will be studied in an integrated room-temperature implosion involving a target with multiple layers.

ACKNOWLEDGMENTS

This material is based upon the work supported by the Department of Energy National Nuclear Security Administration under Award No. DE-NA0001944, the University of Rochester, and the New York State Energy Research and Development Authority. The support of DOE does not constitute an endorsement by DOE of the views expressed in this article.

[1]J. Nuckolls, L. Wood, A. Thiessen, and G. Zimmerman, Nature **239**, 139 (1972).
[2]S. W. Haan, J. D. Lindl, D. A. Callahan, D. S. Clark, J. D. Salmonson, B. A. Hammel, L. J. Atherton, R. C. Cook, M. J. Edwards, S. Glenzer, A. V. Hamza, S. P. Hatchett, M. C. Herrmann, D. E. Hinkel, D. D. Ho, H. Huang, O. S. Jones, J. Kline, G. Kyrala, O. L. Landen, B. J. MacGowan, M. M. Marinak, D. D. Meyerhofer, J. L. Milovich, K. A. Moreno, E. I. Moses, D. H. Munro, A. Nikroo, R. E. Olson, K. Peterson, S. M. Pollaine, J. E. Ralph, H. F. Robey, B. K. Spears, P. T. Springer, L. J. Suter, C. A. Thomas, R. P. Town, R. Vesey, S. V. Weber, H. L. Wilkens, and D. C. Wilson, Phys. Plasmas **18**, 051001 (2011); P. Y. Chang, R. Betti, B. K. Spears, K. S. Anderson, J. Edwards, M. Fatenejad, J. D. Lindl, R. L. McCrory, R. Nora, and D. Shvarts, Phys. Rev. Lett. **104**, 135002 (2010).
[3]M. C. Herrmann, M. Tabak, and J. D. Lindl, Nucl. Fusion **41**, 99 (2001).
[4]Lord Rayleigh, Proc. London Math. Soc. **XIV**, 170 (1883); G. Taylor, Proc. R. Soc. London, Ser. A **201**, 192 (1950).
[5]S. E. Bodner, Phys. Rev. Lett. **33**, 761 (1974); H. Takabe, K. Mima, L. Montierth, and R. L. Morse, Phys. Fluids **28**, 3676 (1985); R. Betti, V. N. Goncharov, R. L. McCrory, P. Sorotokin, and C. P. Verdon, Phys. Plasmas **3**, 2122 (1996).
[6]S. X. Hu, L. A. Collins, V. N. Goncharov, J. D. Kress, R. L. McCrory, and S. Skupsky, Phys. Rev. E **92**, 043104 (2015).
[7]C. J. Randall, J. R. Albritton, and J. J. Thomson, Phys. Fluids **24**, 1474 (1981).
[8]I. V. Igumenshchev, W. Seka, D. H. Edgell, D. T. Michel, D. H. Froula, V. N. Goncharov, R. S. Craxton, L. Divol, R. Epstein, R. Follett, J. H. Kelly, T. Z. Kosc, A. V. Maximov, R. L. McCrory, D. D. Meyerhofer, P. Michel, J. F. Myatt, T. C. Sangster, A. Shvydky, S. Skupsky, and C. Stoeckl, Phys. Plasmas **19**, 056314 (2012).
[9]J. Delettrez, R. Epstein, M. C. Richardson, P. A. Jaanimagi, and B. L. Henke, Phys. Rev. A **36**, 3926 (1987).
[10]P. B. Radha, V. N. Goncharov, T. J. B. Collins, J. A. Delettrez, Y. Elbaz, V. Yu. Glebov, R. L. Keck, D. E. Keller, J. P. Knauer, J. A. Marozas, F. J. Marshall, P. W. McKenty, D. D. Meyerhofer, S. P. Regan, T. C. Sangster, D. Shvarts, S. Skupsky, Y. Srebro, R. P. J. Town, and C. Stoeckl, Phys. Plasmas **12**, 032702 (2005).
[11]T. R. Boehly, D. L. Brown, R. S. Craxton, R. L. Keck, J. P. Knauer, J. H. Kelly, T. J. Kessler, S. A. Kumpan, S. J. Loucks, S. A. Letzring, F. J. Marshall, R. L. McCrory, S. F. B. Morse, W. Seka, J. M. Soures, and C. P. Verdon, Opt. Commun. **133**, 495 (1997).
[12]J. D. Lindl and E. I. Moses, Phys. Plasmas **18**, 050901 (2011).
[13]V. N. Goncharov, O. V. Gotchev, E. Vianello, T. R. Boehly, J. P. Knauer, P. W. McKenty, P. B. Radha, S. P. Regan, T. C. Sangster, S. Skupsky, V. A. Smalyuk, R. Betti, R. L. McCrory, D. D. Meyerhofer, and C. Cherfils-Clérouin, Phys. Plasmas **13**, 012702 (2006).
[14]A. Simon, R. W. Short, E. A. Williams, and T. Dewandre, Phys. Fluids **26**, 3107 (1983).
[15]S. Skupsky, J. A. Marozas, R. S. Craxton, R. Betti, T. J. B. Collins, J. A. Delettrez, V. N. Goncharov, P. W. McKenty, P. B. Radha, T. R. Boehly, J. P. Knauer, F. J. Marshall, D. R. Harding, J. D. Kilkenny, D. D. Meyerhofer, T. C. Sangster, and R. L. McCrory, Phys. Plasmas **11**, 2763 (2004).
[16]M. Hohenberger, P. B. Radha, J. F. Myatt, S. LePape, J. A. Marozas, F. J. Marshall, D. T. Michel, S. P. Regan, W. Seka, A. Shvydky, T. C. Sangster, J. W. Bates, R. Betti, T. R. Boehly, M. J. Bonino, D. T. Casey, T. J. B. Collins, R. S. Craxton, J. A. Delettrez, D. H. Edgell, R. Epstein, G. Fiksel, P. Fitzsimmons, J. A. Frenje, D. H. Froula, V. N. Goncharov, D. R. Harding, D. H. Kalantar, M. Karasik, T. J. Kessler, J. D. Kilkenny, J. P. Knauer, C. Kurz, M. Lafon, K. N. LaFortune, B. J. MacGowan, A. J. Mackinnon, A. G. MacPhee, R. L. McCrory, P. W. McKenty, J. F. Meeker, D. D. Meyerhofer, S. R. Nagel, A. Nikroo, S. Obenschain, R. D. Petrasso, J. E. Ralph, H. G. Rinderknecht, M. J. Rosenberg, A. J. Schmitt, R. J. Wallace, J. Weaver, C. Widmayer, S. Skupsky, A. A. Solodov, C. Stoeckl, B. Yaakobi, and J. D. Zuegel, Phys. Plasmas **22**, 056308 (2015).
[17]P. B. Radha, J. A. Marozas, F. J. Marshall, A. Shvydky, T. J. B. Collins, V. N. Goncharov, R. L. McCrory, P. W. McKenty, D. D. Meyerhofer, T. C. Sangster, and S. Skupsky, Phys. Plasmas **19**, 082704 (2012).
[18]P. B. Radha, C. Stoeckl, V. N. Goncharov, J. A. Delettrez, D. H. Edgell, J. A. Frenje, I. V. Igumenshchev, J. P. Knauer, J. A. Marozas, R. L. McCrory, D. D. Meyerhofer, R. D. Petrasso, S. P. Regan, T. C. Sangster, W. Seka, and S. Skupsky, Phys. Plasmas **18**, 012705 (2011).
[19]C. D. Zhou and R. Betti, Phys. Plasmas **14**, 072703 (2007).
[20]L. Divol, Lawrence Livermore National Laboratory (private communication, 2012); D. A. Callahan, D. E. Hinkel, R. L. Berger, L. Divol, S. N. Dixit, M. J. Edwards, S. W. Haan, O. S. Jones, J. D. Lindl, N. B. Meezan,

Reuse of AIP Publishing content is subject to the terms at: https://publishing.aip.org/authors/rights-and-permissions. Downloaded to IP: 198.125.179.176 On: Tue, 19 Apr 2016 16:35:07

P. A. Michel, S. M. Pollaine, L. J. Suter, R. P. J. Town, and P. A. Bradley, J. Phys.: Conf. Ser. **112**, 022021 (2008).
[21]J. A. Marozas, S. P. Regan, J. H. Kelly, D. D. Meyerhofer, W. Seka, and S. Skupsky, J. Opt. Soc. Am. B **19**, 7 (2002).
[22]V. N. Goncharov, T. C. Sangster, R. Betti, T. R. Boehly, M. J. Bonino, T. J. B. Collins, R. S. Craxton, J. A. Delettrez, D. H. Edgell, R. Epstein, R. K. Follet, C. J. Forrest, D. H. Froula, V. Yu. Glebov, D. R. Harding, R. J. Henchen, S. X. Hu, I. V. Igumenshchev, R. Janezic, J. H. Kelly, T. J. Kessler, T. Z. Kosc, S. J. Loucks, J. A. Marozas, F. J. Marshall, A. V. Maximov, R. L. McCrory, P. W. McKenty, D. D. Meyerhofer, D. T. Michel, J. F. Myatt, R. Nora, P. B. Radha, S. P. Regan, W. Seka, W. T. Shmayda, R. W. Short, A. Shvydky, S. Skupsky, C. Stoeckl, B. Yaakobi, J. A. Frenje, M. Gatu-Johnson, R. D. Petrasso, and D. T. Casey, Phys. Plasmas **21**, 056315 (2014).
[23]J. A. Marozas, F. J. Marshall, R. S. Craxton, I. V. Igumenshchev, S. Skupsky, M. J. Bonino, T. J. B. Collins, R. Epstein, V. Yu. Glebov, D. Jacobs-Perkins, J. P. Knauer, R. L. McCrory, P. W. McKenty, D. D. Meyerhofer, S. G. Noyes, P. B. Radha, T. C. Sangster, W. Seka, and V. A. Smalyuk, Phys. Plasmas **13**, 056311 (2006).
[24]D. Cao, G. Moses, and J. Delettrez, Phys. Plasmas **22**, 082308 (2015).
[25]D. H. Edgell, P. B. Radha, V. N. Goncharov, I. V. Igumenshchev, J. A. Marozas, J. F. Myatt, W. Seka, and D. H. Froula, Bull. Am. Phys. Soc. **57**, 343 (2012).
[26]D. E. Bower, T. J. McCarville, S. S. Alvarez, L. E. Ault, M. D. Brown, M. P. Chrisp, C. M. Damian, W. J. DeHope, D. H. Froula, S. H. Glenzer, S. E. Grace, K. Gu, F. R. Holdener, C. K. Huffer, J. H. Kamperschroer, T. M. Kelleher, J. R. Kimbrough, R. Kirkwood, D. W. Kurita, A. P. Lee, F. D. Lee, I. T. Lewis, F. J. Lopez, B. J. MacGowan, M. W. Poole, M. A. Rhodes, M. B. Schneider, N. R. Sewall, F. Y. Shimamoto, S. J. Shiromizu, D. Voloshin, A. L. Warrick, C. R. Wendland, and B. K. Young, Rev. Sci. Instrum. **75**, 4177 (2004); J. D. Moody, P. Datte, K. Krauter, E. Bond, P. A. Michel, S. H. Glenzer, L. Divol, C. Niemann, L. Suter, N. Meezan, B. J. MacGowan, R. Hibbard, R. London, J. Kilkenny, R. Wallace, J. L. Kline, K. Knittel, G. Frieders, B. Golick, G. Ross, K. Widmann, J. Jackson, S. Vernon, and T. Clancy, Rev. Sci. Instrum. **81**, 10D921 (2010); P. Datte, A. M. Manuel, M. Eckart, M. Jackson, H. Khater, and M. Newton, "Target diagnostics physics and engineering for inertial confinement fusion II," Proc. SPIE **8850**, 885003 (2013).
[27]D. T. Michel, C. Sorce, R. Epstein, N. Whiting, I. V. Igumenshchev, R. Jungquist, and D. H. Froula, Rev. Sci. Instrum. **83**, 10E530 (2012).
[28]F. J. Marshall, P. W. McKenty, J. A. Delettrez, R. Epstein, J. P. Knauer, V. A. Smalyuk, J. A. Frenje, C. K. Li, R. D. Petrasso, F. H. Séguin, and R. C. Mancini, Phys. Rev. Lett. **102**, 185004 (2009).
[29]J. J. MacFarlane, I. E. Golovkin, P. Wang, P. R. Woodruff, and N. A. Pereyra, High Energy Density Phys. **3**, 181 (2007).
[30]See National Technical Information Service Document No. PB2006-106662 [LLE Review Quarterly Report **91**, 116 (2002), Laboratory for Laser Energetics, University of Rochester, Rochester, NY, LLE Document No. DOE/SF/19460-458]. Copies may be obtained from the National Technical Information Service, Springfield, VA.
[31]G. Fiksel, S. X. Hu, V. N. Goncharov, D. D. Meyerhofer, T. C. Sangster, V. A. Smalyuk, B. Yaakobi, M. J. Bonino, and R. Jungquist, Phys. Plasmas **19**, 062704 (2012); S. X. Hu, G. Fiksel, V. N. Goncharov, S. Skupsky, D. D. Meyerhofer, and V. A. Smalyuk, Phys. Rev. Lett. **108**, 195003 (2012).
[32]A. N. Mostovych, D. G. Colombant, M. Karasik, J. P. Knauer, A. J. Schmitt, and J. L. Weaver, Phys. Rev. Lett. **100**, 075002 (2008).
[33]R. C. Malone, R. L. McCrory, and R. L. Morse, Phys. Rev. Lett. **34**, 721 (1975); J. Delettrez, Can. J. Phys. **64**, 932 (1986).
[34]M. Hohenberger, F. Albert, N. E. Palmer, J. J. Lee, T. Döppner, L. Divol, E. L. Dewald, B. Bachmann, A. G. MacPhee, G. LaCaille, D. K. Bradley, and C. Stoeckl, Rev. Sci. Instrum. **85**, 11D501 (2014).
[35]B. Yaakobi, A. A. Solodov, J. F. Myatt, J. A. Delettrez, C. Stoeckl, and D. H. Froula, Phys. Plasmas **20**, 092706 (2013).
[36]J. A. Delettrez, T. J. B. Collins, and C. Ye, Bull. Am. Phys. Soc. **59**, 150 (2014).
[37]T. J. Murphy, N. S. Krasheninnikova, G. A. Kyrala, P. A. Bradley, J. A. Baumgaertel, J. A. Cobble, P. Hakel, S. C. Hsu, J. L. Kline, D. S. Montgomery, K. A. D. Obrey, R. C. Shah, I. L. Tregillis, M. J. Schmitt, R. J. Kanzleiter, S. H. Batha, R. J. Wallace, S. D. Bhandarkar, P. Fitzsimmons, M. L. Hoppe, A. Nikroo, M. Hohenberger, P. W. McKenty, H. G. Rinderknecht, M. J. Rosenberg, and R. D. Petrasso, Phys. Plasmas **22**, 092707 (2015); N. S. Krasheninnikova, J. A. Cobble, T. J. Murphy, I. L. Tregillis, P. A. Bradley, P. Hakel, S. C. Hsu, G. A. Kyrala, K. A. Obrey, M. J. Schmitt, J. A. Baumgaertel, and S. H. Batha, *ibid.* **21**, 042703 (2014).
[38]T. J. Murphy, Los Alamos National Laboratory, private communication (2015).
[39]F. Weilacher, P. B. Radha, T. J. B. Collins, and J. A. Marozas, Phys. Plasmas **22**, 032701 (2015); D. Cao, J. A. Marozas, T. J. B. Collins, P. B. Radha, and P. W. McKenty, "A new intermediate far-field spot design for polar direct drive at the National Ignition Facility," Bull. Am. Phys. Soc. **60**, 29 (2015).
[40]A. R. Christopherson, R. Betti, W. Theobald, and J. Howard, "probing hot electron preheat and hot spot asymmetries in ICF Implosions," paper presented at the Ninth International Conference on Inertial Fusion Sciences and Applications (IFSA 2015), Seattle, WA, 20–25 September 2015 (Paper Th.O.2.2).
[41]"Cryogenic deuterium and deuterium–tritium direct-drive implosions on OMEGA," in LLE Review Quarterly Report **130**, 72 (2012), edited by A. Shvydky, Laboratory for Laser Energetics, University of Rochester, Rochester, NY, LLE Document No. DOE/NA/28302-1058, available at http://www.lle.rochester.edu/media/publications/lle_review/documents/v130/130_02_Cryogenic.pdf.
[42]See National Technical Information Service Document No. DE2002762802 [LLE Review Quarterly Report **79**, 121 (1999), Laboratory for Laser Energetics, University of Rochester, Rochester, NY, LLE Document No. DOE/SF/19460-317]. Copies may be obtained from the National Technical Information Service, Springfield, VA.
[43]W. Seka, D. H. Edgell, J. F. Myatt, A. V. Maximov, R. W. Short, V. N. Goncharov, and H. A. Baldis, Phys. Plasmas **16**, 052701 (2009).
[44]M. Hohenberger, A. Shvydky, P. B. Radha, M. J. Rosenberg, V. N. Goncharov, F. J. Marshall, J. P. Knauer, S. P. Regan, T. C. Sangster, A. Nikroo, and R. J. Wallace, Bull. Am. Phys. Soc. **60**, 164 (2015); A. Shvydky, M. Hohenberger, P. B. Radha, M. J. Rosenberg, R. S. Craxton, V. N. Goncharov, J. A. Marozas, F. J. Marshall, P. W. McKenty, S. P. Regan, and T. C. Sangster, Bull. Am. Phys. Soc. **60**, 118 (2015).
[45]J. A. Marozas, T. J. B. Collins, J. D. Zuegel, P. B. Radha, F. J. Marshall, and W. Seka, "Cross-Beam Energy Transfer Mitigation Strategy for NIF Polar Drive," paper presented at the 44th Annual Anomalous Absorption Conference, Estes Park, CO, 8−13 June 2014.
[46]D. T. Michel, V. N. Goncharov, I. V. Igumenshchev, R. Epstein, and D. H. Froula, Phys. Rev. Lett. **111**, 245005 (2013).

Reuse of AIP Publishing content is subject to the terms at: https://publishing.aip.org/authors/rights-and-permissions. Downloaded to IP: 198.125.179.176 On: Tue, 19 Apr 2016 16:35:07